European Journal of Environmental and Civil Engineering

Volume 26 Number 3 February 2022

Editors-in-chief
Günther Meschke
François Nicot

Taylor & Francis

ISSN: (Print) (Online) Journal homepage: https://www.tandfonline.com/loi/tece20

Multicycle expansion tests in natural soils

Essais d'expansion multicycle dans les sols en place

P.-G. Karagiannopoulos, Q.-H. Dang, P. Reiffsteck, J. Benoît, J.-C. Dupla & M. Peronne

To cite this article: P.-G. Karagiannopoulos, Q.-H. Dang, P. Reiffsteck, J. Benoît, J.-C. Dupla & M. Peronne (2022): Multicycle expansion tests in natural soils, European Journal of Environmental and Civil Engineering, DOI: 10.1080/19648189.2022.2030805

To link to this article: https://doi.org/10.1080/19648189.2022.2030805

Published online: 10 Mar 2022.

EUROPEAN JOURNAL OF ENVIRONMENTAL AND CIVIL ENGINEERING
https://doi.org/10.1080/19648189.2022.2030805

Multicycle expansion tests in natural soils
Essais d'expansion multicycle dans les sols en place

P.-G. Karagiannopoulos[a,b], Q.-H. Dang[b,c], P. Reiffsteck[b], J. Benoît[d], J.-C. Dupla[e] and M. Peronne[a]

[a]Jean Lutz SA, Jurancon, NA, France; [b]Université Gustave Eiffel, Champs sur Marne, France; [c]Hanoi University of Mining and Geology, Hanoi, Vietnam; [d]University of New Hampshire, Durham, NH, USA; [e]Navier Laboratory, Ecole Nationale des Ponts et Chaussées, Marne-la-Vallée, France

ABSTRACT

This paper presents an application of multicyclic expansion tests carried out with a pressuremeter at two experimentation sites to evaluate soil susceptibility to this type of solicitation. These unique pressuremeter tests, interpreted in terms of deformation (volume change or radial strain) and number of cycles, offer relationships as a function of cyclic shear ratio. New test procedures and probe enhancements were also implemented to develop additional data and to improve the quality of these tests. These cyclic tests were performed using a pre-bored Ménard pressuremeter as well as a new pressuremeter probe equipped with a miniature pore pressure transducer. Two sites were studied, one located in French Antilles and the second one located in Brittany (France), both consisting of normally consolidated sandy and silty soils profiles. An estimation of the relationship between cyclic stress ratio applied during the tests and the number of cycles to reach failure are presented and discussed in this paper. These results were compared to traditional cyclic laboratory test results and showed great potential for this in situ testing method. The results were used to develop preliminary charts for liquefaction prediction. This article presents a summary of the analysis and application of these cyclic pressuremeter tests.

ARTICLE HISTORY
Received 31 August 2021
Accepted 12 January 2022

KEYWORDS
Multicyclic test; cyclic stress ratio; in situ tests; pressuremeter test; calibration chamber; excess pore pressures

1. Introduction

Determination of the cyclic resistance potential of soils is of significant importance to safeguard structures against damages and/or failures during earthquakes. Since the Niigata, Alaska, and Kobe earthquakes, several research groups have developed, tested and validated various methods to evaluate this phenomenon. These efforts have primarily focused on laboratory tests in which conditions such as density, fines content, stress history, confining pressure and stress paths are controlled and can be used to evaluate the effect of various parameters (Bray & Sancio, 2006; Ishihara, 1993; Ueno et al., 2015).

Laboratory tests overwhelmingly rely on reconstituted samples because of the difficulties involved in obtaining undisturbed samples of granular soils. Although some techniques exist to sample soils with minimal disturbance such as freezing and impregnation methods, those are not routinely used because of cost and complexity (Ferreira et al., 2020). Granular soils with plastic or non-plastic fines are also very difficult to reconstitute in the laboratory to conditions identical to those in situ. These sampling and specimen preparation drawbacks have led to an increased interest in field testing techniques.

CONTACT P. Reiffsteck philippe.reiffsteck@univ-eiffel.fr Université Gustave Eiffel, 14-19 Blvd. Newton, Champs sur Marne, IdF 77447, France.

Depending on the method of insertion into the ground (pre-bored, self-bored or pushed-in), the pressuremeter is considered the reference test to determine the in situ horizontal stress state and can provide a complete stress-strain curve during the test (Benoît et al., 2020). With minor modifications and improved data acquisition systems, the pressuremeter can also be used for cyclic loading in which amplitude and frequency can be varied (Dupla & Canou, 2003; Jézéquel & Le Méhauté, 1982). The interest of performing unload-reload loops with the pressuremeter to obtain the elastic modulus appeared very early in the work of Ménard (1960). With a sufficient number of cycles, it is possible to observe pore pressure increases or the equivalent volume changes up to liquefaction (Dupla & Canou, 2003). Overall, these various improvements suggest that the pressuremeter is well-suited for evaluating liquefaction potential in situ.

The primary objective of the work presented in this paper is to show the potential of a specially modified pre-bored pressuremeter and upgraded control system to perform high quality cyclic testing to study liquefaction in situ. This paper presents the pressuremeter modifications and its application to study the resistance of soil to cyclic solicitation. The field results are compared to those from laboratory testing.

1.1. First approach

The pressuremeter test, initially developed by Ménard in the 1960s, consists in lowering a cylindrical probe covered with a rubber membrane into a pre-bored hole, and inflating the membrane in increments of pressure until the cavity has approximately doubled in volume. The test and its procedures are well-documented in the literature (ASTM, 2020; ISO, 2004).

Cyclic tests using the pressuremeter have also been used since the early introduction of the technique. These tests included one or more unloading-reloading loop making it possible to determine cyclic deformation moduli as a function of stress level. The values obtained are somewhere between the moduli measured in small strain from dynamic laboratory tests or with in situ seismic wave propagation tests and the conventional Ménard modulus evaluated along the quasi-elastic phase of the expansion test (Ménard, 1960; Tani, 1995; Tatsuoka et al., 1997). These cyclic tests are mainly intended to 'erase' the initial disturbance from predrilling along the borehole cavity wall (AFNOR, 1999; Combarieu & Canépa, 2001) to provide a more appropriate elastic response of the soil. However, Dupla and Canou (2003) found that a single cycle of unload-reload is insufficient to identify changes in soil characteristics under cyclic loading.

During the 1970s, the Association for Research in Marine Geotechnics (ARGEMA) in France, brought together several consultants and research agencies dealing with offshore geotechnical issues and conducted a multi-site cyclic pressuremeter test program. The details of the experiments are summarized in several reports and articles in the proceedings of the Symposium on the Pressuremeter and its Marine Applications held in 1982 in Paris (Jézéquel & Le Méhauté, 1982). As documented in these references, the cyclic expansion tests were carried out to assist in the design of offshore platform piles. The tests were preferably performed using self-boring pressuremeter probes.

Other researchers such as Masuda et al. (2005, 2008) also used the cyclic pressuremeter testing to liquefy soils in situ. Such tests required a very sophisticated and unique probe composed of five cells that were alternately inflated in order to shear the soil at mid-plane. The measurement of the interstitial pressure was carried out on the central section. The few trials that have been published show a good relationship between number of cycles and the increase in pore water pressure.

The use of the conventional pressuremeter for liquefaction studies started as early as 1995 by Dupla (1995). Although, the idea of cyclic testing during pressuremeter tests appeared very early for evaluating soil-structure interaction in offshore foundations (Jézéquel & Le Méhauté, 1982; Little & Briaud, 1988), the use of the pressuremeter for liquefaction originated from Dupla (1995).

Dupla (1995) carried out several expansion tests in a thick cylinder and in a calibration chamber with a mini pressuremeter (diameter of 32 mm). Figure 1 shows some of the results in terms of volume change variation with the number of cycles for four relative densities ($I_d = (e_{max} - e)/(e_{max} - e_{min})$). The trend of the experimental accumulation curves follows a power law (Figure 2b).

Figure 2 compares the results obtained by Dupla (1995) during these cyclic pressuremeter tests (cPMT) to the results of cyclic triaxial tests (cTXT) conducted by Gobbi (2020) and those from Dupla (1995).

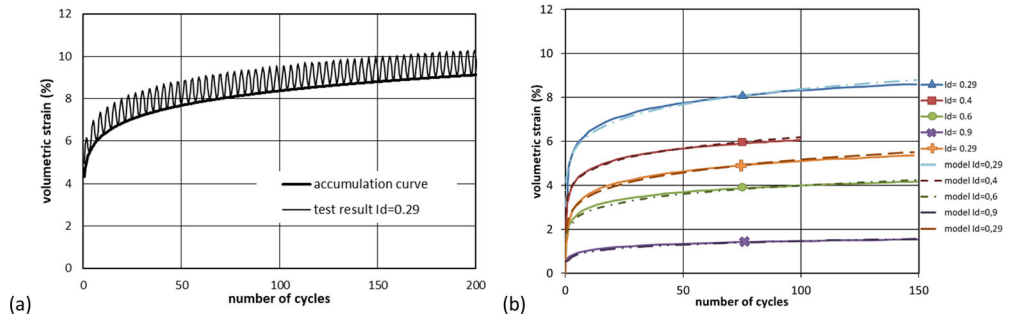

Figure 1. Mini cyclic pressuremeter tests after Dupla (1995).

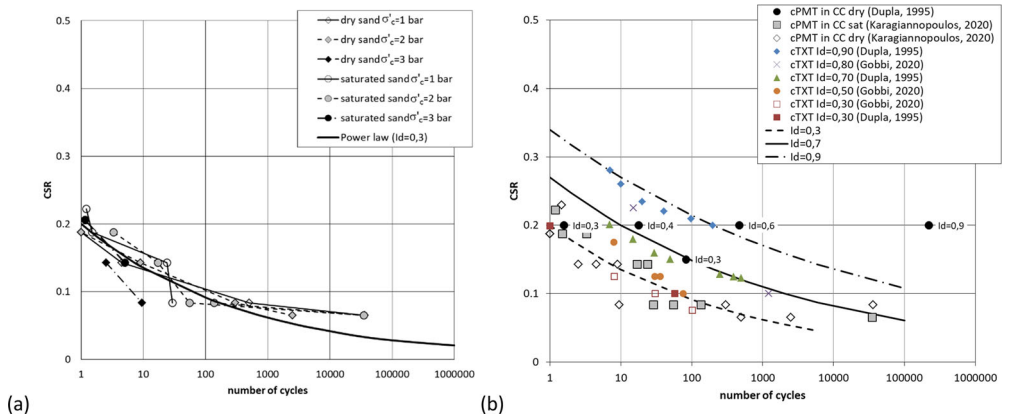

Figure 2. Synthesis of laboratory and calibration chamber tests on Hostun sand (a) 44 mm probe (Karagiannopoulos, 2020) and (b) all probes.

Figure 2b compares the results from calibration chamber tests for a 32 mm monocell probe (cPMT in CC dry) with the reconstituted sand around the probe at a 5% volumetric strain ($\varepsilon_V = \Delta V/V_0$) accumulation to the Ishihara failure criterion from the laboratory tests which considers a double amplitude axial deformation of 5% (Ishihara, 1993). The results obtained in the calibration chamber show a close agreement to the curve determined from laboratory tests for the low values of density index but more distant for higher values. A new series of tests in calibration chamber has been performed by Karagiannopoulos using a 44 mm tricell probe in Hostun sand for a density index I_d=0.3 in dry and saturated conditions (2020). These results showed that using the 5% volumetric strain criteria led to the same trend in both drained and undrained conditions (Figure 1a).

2. Equipment improvements

2.1. Pressuremeter

The basic principle of the pressuremeter test is to measure pressure-deformations or volume changes during cavity expansion. For this research project, each test consisted of several cycles of loading-unloading during the expansion test to simulate the effect of repeated loading or dynamic events. These cavity expansion cyclic tests can be performed with any pressuremeter probe with any insertion procedures such as self-boring, pre-boring or static penetration. The Ménard pressuremeter test equipment used in this project allowed operators to achieve monotonic expansion tests (EN ISO 22476-4 similar to ASTM D4719) and cyclic tests (NF P94-110-2) (ASTM, 2020; AFNOR, 1999; ISO, 2004). These tests included unload-reload cycles performed in steps using the same test procedures as outlined for the Ménard pressuremeter test described in the EN ISO 22476-4 standard. The probe used for this testing program was a standard Ménard tri-cell probe. The tests were carried out using a pressure volume control unit (PVCU)

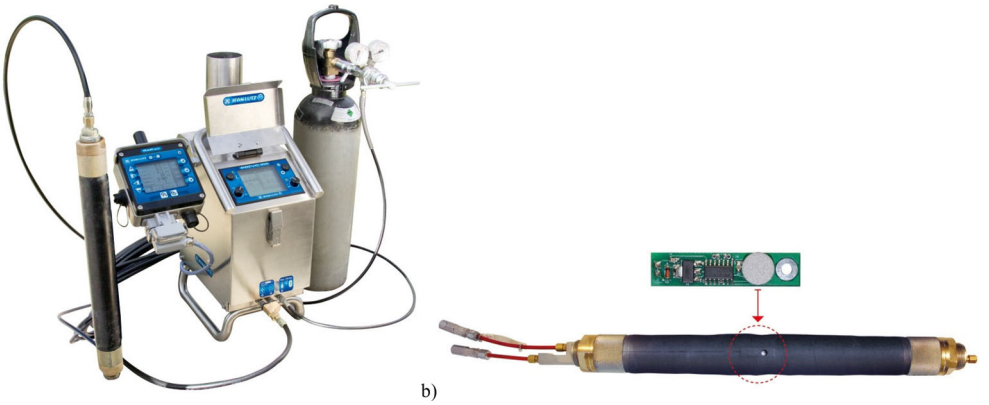

Figure 3. photograph (a) of cyclic Ménard pressuremeter test equipment and (b) Pore pressure transducer attached to the flexible membrane cover.

and datalogger equipment manufactured by Jean Lutz SA. The system, shown in Figure 3a, is connected to a portable computer which controls every aspects of the test using a series of solenoid valves as well as pressure transducers and flowmeters. The testing procedures are carried out automatically either directly on the control unit or using a software program developed by Jean Lutz. The probe expansion is measured by recording the volume changes during the various pressure increments.

Evaluation of excess pore pressures during cavity expansion has been shown to be of significant importance in liquefaction studies (Bensaïd, 1985). Although some self-boring pressuremeters are equipped with pore pressure sensors, the conventional Ménard pressuremeter only measures the pressure-volume response of the soil. Laboratory experiments have shown that soil liquefaction initiates when the pore pressure increases to a value close to the confining pressure at which point the effective stress becomes zero. Consequently, it is important to measure pore pressures during cyclic expansion in order to estimate the liquefaction potential of soils. The pressuremeter used for this project was specially equipped with one pore pressure transducer fixed on the outside of the expanding rubber membrane as shown in Figure 3b. The transducer is glued on the membrane and powered using a thin wire embedded in a shallow groove in the membrane. The wire runs up to the surface along the pressuremeter tubing.

Preliminary tests were carried out with a Cambridge Insitu self-boring pressuremeter equipped with two pore pressure sensors (A and B) diametrically opposed using the control system described previously. The tests were performed in a soft marine clay deposit at the New Hampshire seacoast, USA. Figure 4 shows a typical response from the pore pressure sensors under cyclic pressuremeter loading. It can observe that changes in total stress generate an immediate response of pore pressures during cyclic loading.

Using the experience gained at the New Hampshire test site, a simple and robust transducer that can be fixed directly on the membrane was developed for use on the standard pressuremeter probe. The first prototype tests were carried out on Le Sillon dyke located in the city of Saint Malo, France. The results presented on Figure 5 suggest that the permeable sand at the site allowed the pore pressures to dissipate rapidly. The response of the pore pressure sensor clearly shows its potential for measuring pore pressure development during cyclic loading as demonstrated previously at the Dover, NH site.

2.2. Membrane stiffness correction

Depending on the type of pressuremeter, membrane type and soil to be tested, the pressure losses due to membrane stiffness must be properly taken into account to get accurate soil pressure-volume change measurements. The pressure loss correction accounts for the increase of resistance due to membrane stiffness during expansion (ASTM, 2020; ISO, 2004). The correction is obtained by expanding the membrane in air. Figure 6 shows various membrane expansion curves in air for different membrane configurations: rubber, metal sheath with membrane, canvas, rubber with canvas, slotted tube and slotted casing. The figure illustrates the importance of this calibration especially in soft soils where the stiffness of the membrane is significant with respect to the actual soil resistance. The correction for membrane stiffness

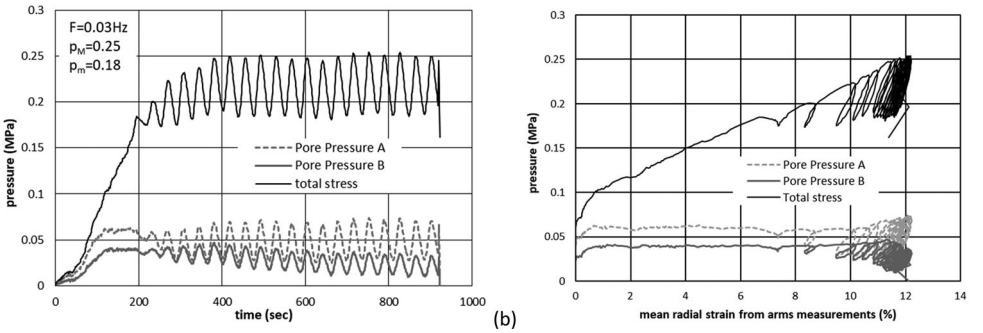

Figure 4. Measure of pore pressure in self-boring pressuremeter tests (Dover, NH site).

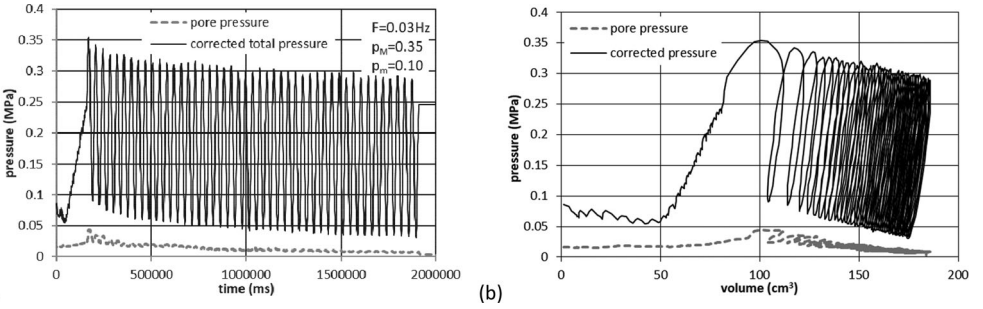

Figure 5. Measure of pore pressure in pre-bored pressuremeter tests (Le Sillon, Saint Malo site).

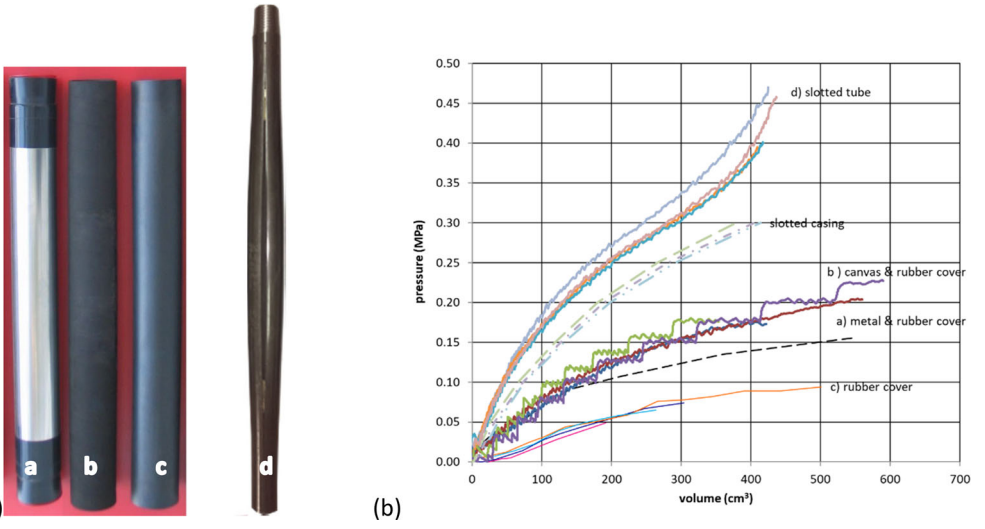

Figure 6. Membranes and correction curves for different membrane cover systems.

is usually performed on the pressure-volume test curve after the test has been completed as part of the analysis of the pressuremeter test measurements. However, for cyclic pressuremeter tests, it is critical to correct for membrane stiffness during the application of the loading and unloading cycles. The cyclic loading program allows the user to define any type of loading signal (e.g. harmonic or multiple frequencies) and to account for the membrane stiffness throughout the test.

Figure 7 illustrates the importance of membrane stiffness correction during the test. The lighter grey curves show the intended loading cycles which should vary between p_m and p_M. However, for properly correcting for membrane inertia, the applied pressure has to increase with each cycle an amount

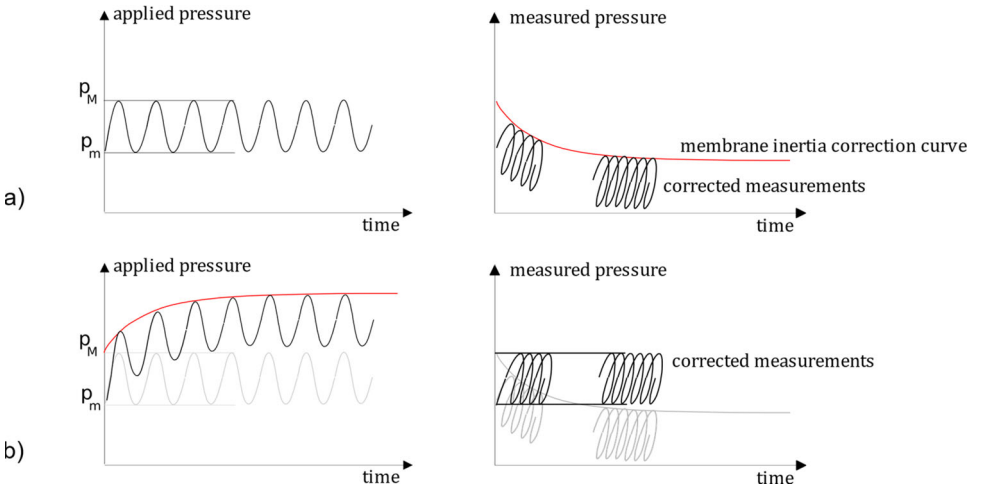

Figure 7. Loading pressuremeter test program to account for membrane stiffness (a) loading program without integration of correction curve and results obtained (b) loading program modified and results.

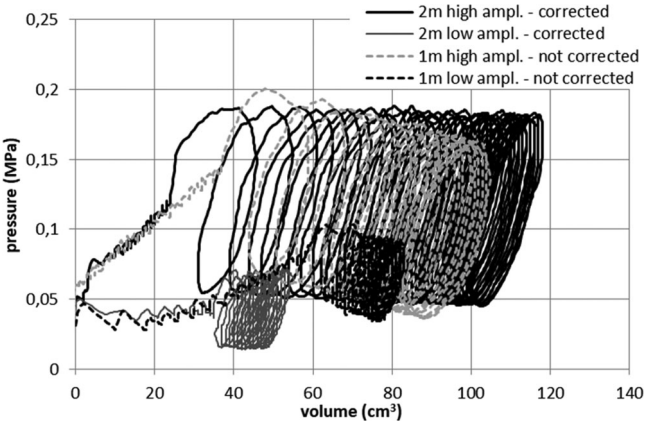

Figure 8. Comparison of test results with corrected loading program (Plancöet site).

equivalent to the membrane stiffness (Figure 7a). Examples of such application of instantaneous membrane inertia corrections are shown schematically on Figure 7b and on an actual cyclic pressuremeter test in Plancöet (France) on Figure 8. These corrections are applied in real-time resulting in a corrected curve that appropriately cycles between the intended pressure amplitudes as shown by the constant pressure amplitudes with increasing volume.

3. Testing procedures

Each pressuremeter test holes were cased down through surficial fills, if any, and then hand-augered using bentonite mud to each test depths. When a slotted tube was used to protect the rubber membrane, the probe was lowered in a pre-drilled hole advanced with a continuous flight auger of the same diameter. In general, the boreholes were advanced in 1-meter depth increment to minimize borehole relaxation and disturbance (Reiffsteck et al., 2020). For tests using a slotted tube probe, each advance did not exceed three meters. Tests were performed below the ground water table level in a borehole full of flushing medium. Saturation conditions were kept close as possible to their initial state. In this paper, no corrections were made to account of a potential difference in the saturation quality compared to triaxial and calibration chamber tests used as reference (Vernay et al., 2020).

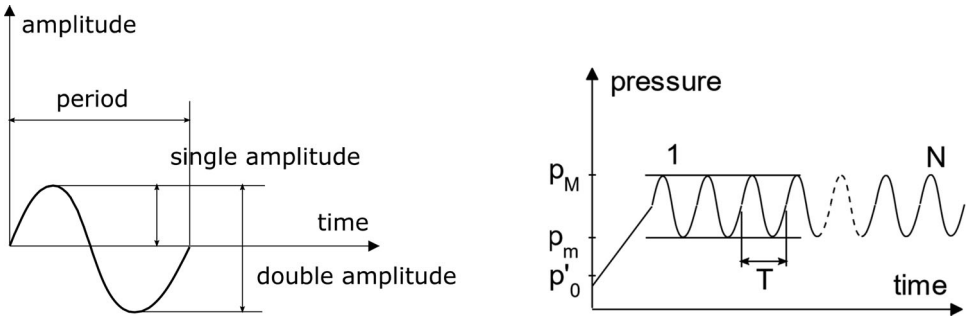

Figure 9. Definition of cyclic test parameters.

In this research, the cycles were applied according to a harmonic signal with a predefined pressure-control rate without incremental steps as shown in Figure 9. A single loading program was used which consisted in cyclically loading between two pressure limits, p_M and p_m. All cyclic parameters are defined on the figure.

The tests were carried out in pressure-controlled mode with a cyclic frequency based on soil type using a predefined stress level. The duration of the cycle was chosen so that the cyclic stress remained rapid enough to observe the dynamic response of the soil in almost undrained conditions (especially in impervious soil) but also taking into account the reaction time of the control unit (PVCU). A parametric laboratory triaxial tests study with cyclic frequency varying between 0.005 and 2.0 Hz has shown the need to keep the cyclic loading frequency greater than 0.01 to avoid potential overestimation of the number of cycle to reach liquefaction (Gobby, 2020). Therefore, in this testing program the cycle frequencies were kept between 0.01 and 0.05 Hz. The number of cycles N was limited to 50 for potential use in daily practice. An initial monotonic loading with a total duration of 160 s was also included to reach the mean pressure $P_{av} = (p_M + p_m)/2$. The cavity pressure was varied according to a sinusoidal signal as described in Eq. (1).

$$p_{cav} = \frac{p_M + p_m}{2} \cdot \left(1 + \frac{p_M - p_m}{p_M + p_m} \cdot \sin(\omega \cdot t)\right) \tag{1}$$

With $\omega = {}^{2\cdot\pi}/_{T}$ and T the signal period in seconds.

The initial pressure p_m which defines the lower limit of the cycles was kept greater than the horizontal effective stress $\sigma_h{}'_0$ so that the probe is always remain in contact with the surrounding borehole wall while the maximum pressure p_M is selected to obtain a specific stress ratio as defined by Dupla and Canou (2003). The pressure σ'_{h0} was estimated from previous Ménard type expansion test results using the minimum curvature point as the probe re-contacts the borehole wall (Benoît et al., 2020).

3.1. Data analysis

Using the results from cyclic triaxial tests, the Cyclic Stress Ratio (CSR), conventionally defined as the ratio of the maximum cyclic deviatoric stress over twice the initial effective confining stress, σ'_c, as shown in Eq. (2) was used as the basis for a similar CSR for the pressuremeter test:

$$CSR_{TXT} = \frac{\delta(\sigma_1 - \sigma_3)_{cy}}{2 \cdot \sigma'_c} \tag{2}$$

In the triaxial test, the failure can be generally defined as the onset of liquefaction where the excess pore pressure Δu is equal to σ'_c ($r_u = \Delta u/\sigma'_c = 1$) or, at a double amplitude axial deformation of 5% (Ishihara, 1993). For the pressuremeter test, the Cyclic Stress Ratio is defined similarly as the ratio of the simple cyclic amplitude $\delta(\tau_e)_{cy}$ of shear stress over the mean horizontal stress, $\sigma_{H;mean}$, during the test as shown in Eq. (3):

$$CSR_{PMT} = \frac{\delta(\tau_e)_{cy}}{\sigma_{H;mean}} = \frac{\delta(\sigma_r - \sigma_\theta)_{cy}}{2 \cdot \sigma_{H;mean}} \tag{3}$$

At an early stage of the test, in small strain, when soil can be considered elastic, the increment of circumferential stress $\delta\sigma_\theta$ is equal to the increment of radial stress $\delta\sigma_r$ but for larger strain in loose granular

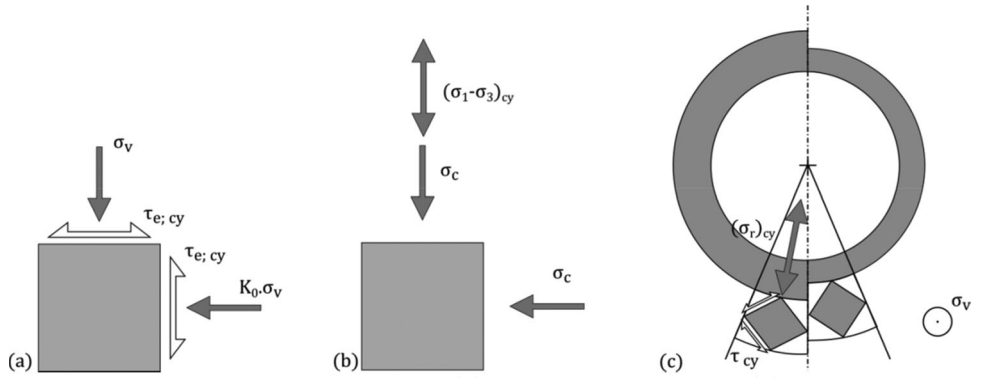

Figure 10. Comparison of stresses in situ during earthquake (a), during a cyclic triaxial test (b) and during a cyclic pressuremeter test (c) (modified from Castro, 1975).

material the increment of deviatoric stress is equal to the radial stress as the circumferential stress become negligible (i.e. $\delta\sigma_\theta \cong 0$). This has been observed by Mokrani (1991) in calibration chamber.

Hence at large strain,

$$CSR_{PMT} = \frac{\delta(\sigma_r)_{cy}}{2 \cdot \sigma_{H;mean}} = \frac{\frac{p_M - p_m}{2}}{2 \cdot \left(\frac{p_M + p_m}{2}\right)} = \frac{p_M - p_m}{2 \cdot (p_M + p_m)} \tag{4}$$

According to Castro (1975), during a laboratory cyclic triaxial test (i.e. $\sigma_2 = \sigma_3$) the criteria can be expressed as shown in Eq. (5) and in Figure 10:

$$\frac{\tau_{oct}}{\sigma_{oct}} = \frac{2 \cdot \sqrt{2}}{3} \cdot \frac{\sigma_1 - \sigma_3}{2 \cdot \sigma_c} \tag{5}$$

and in the field during a seismic event:

$$\frac{\tau_{oct}}{\sigma_{oct}} = \frac{\sqrt{6}}{1 + 2 \cdot K_0} \cdot \frac{\tau_e}{\sigma_v} \tag{6}$$

During the pressuremeter test, the cyclic shear stress imposed to the soil close to the probe is applied in the horizontal plane and the initial vertical and horizontal stresses are identical as in the earthquake conditions (Figure 10). Consequently, the same formula (6) may be used.

Based on this analysis, the CSR imposed in situ must be corrected by a factor reflecting the stress path applied to reach the conventional liquefaction (Eq. (7)).

From the equality of Eqs. (5) and (6) we can deduce:

$$CSR_{Field} = CSR_{PMT} = \frac{\tau_\varepsilon}{\sigma_v} = \frac{2 \cdot (1 + 2 \cdot K_0)}{3 \cdot \sqrt{3}} \cdot \frac{\sigma_1 - \sigma_3}{2 \cdot \sigma_c} = \frac{2 \cdot (1 + 2 \cdot K_0)}{3 \cdot \sqrt{3}} \cdot CSR_{TXT} \tag{7}$$

Which gives for a sand a value close to 0.71 for a friction angle of 35°, and 0.87 for a silt with a friction angle of 22°, using K_0 estimated using the Jaky (1944) formula. In tests performed in calibration chamber by Dupla (1995), and Karagiannopoulos (2020) an isotropic consolidation state was imposed leading to a correlation between CSR_{TXT} et CSR_{PMT} close to 1.15 (Figure 2).

As presented on Figure 11, the pressuremeter tests are carried out at different stress amplitudes Δp, and the resulting CSR evolution curves are plotted against the number of cycles N to failure. During a cyclic pressuremeter test, failure is defined in a similar way to the triaxial test. In Figure 11, N_L corresponds to the number of cycles to liquefaction, ε_r is the radial strain calculated from the volume change and r_u is the pore pressure ratio. Unlike for the laboratory experiments such as the triaxial test or the simple shear test, for *in situ* tests it is not possible to change or modify the soil density so the tests are carried out at the existing in place density and amplitude has to be varied accordingly to reach the CSR values. When pore pressure measurements are available, the failure is defined using $r_u = 1$ as shown for the first two cases on Figure 11.

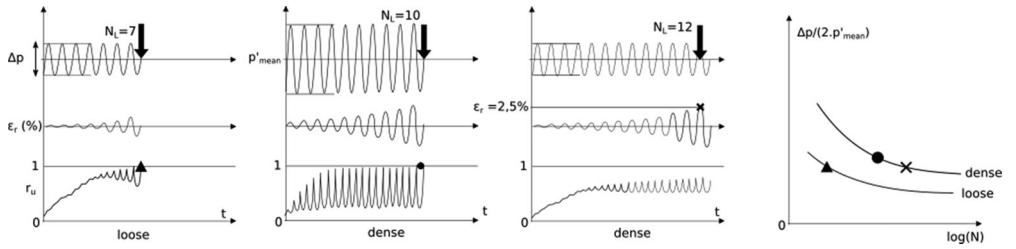

Figure 11. Pressuremeter cyclic behavior and CSR concept (modified from Ishihara, 1993).

To obtain the radial strain ε_r, it requires transforming the measured volume changes during the pressuremeter expansion into volumetric strains (Eqs. (8) and (9)).

$$\varepsilon_V = \frac{\Delta V}{V_0} = \frac{V - V_0}{V_0} \tag{8}$$

where: V = measured current cavity volume during the test
V_0 = initial cavity volume
and

$$\varepsilon_r = \sqrt{\varepsilon_V + 1} - 1 \tag{9}$$

For cases when only volume changes are recorded, Dupla (1995) proposed to use the envelope of volume versus number of cycles fitted with a power law to define the failure for a given ε_r. For the *in situ* pre-bored pressuremeter testing, the probe placement is different from the calibration chamber where the soil is 'molded' around the probe. This slightly remolded zone resulting in volume accumulation during the preliminary loading phase. In addition, the drainage conditions may induce some dissipation of the pore pressure takes place during the cycling which further increases the cavity volumetric strain as compared to the behavior in the equivalent triaxial tests. As a result, a failure criterion with a higher volumetric strain such as $\varepsilon_v = 50\%$ has been proposed in order to obtain a number of cycles comparable to the cyclic cavity expansion laboratory tests (calibration chamber, thick cylinder).

3.2. In situ testing program

Testing using the cyclic pressuremeter was conducted at two field sites at different stages of improvements to the probe and testing protocols. The first site was on the eastern part of Guadeloupe (Gosier) with a standard pressuremeter probe without pore pressure measurement capabilities. The second site was in Brittany, France (Saint Benoit-des-Ondes) and the testing was carried out with a probe equipped with pore pressure sensors and the applied load cycles were corrected in real-time for membrane inertia and stiffness. The following sections present basic soil profiles and geotechnical properties for both sites. More details can be found in Dupla and Canou (2010), Dang (2019) and Karagiannopoulos (2020). Details regarding these tests are summarized in Table 1. Indices are used in Table 1 for the 2018 and 2019 campaigns to distinguish the different applied cyclic ratios (CSR) at the same depth. The membrane stiffness correction was applied only in the 2019 Saint Benoit des Ondes campaign. All pressure values (P_M, P_m) are corrected and for this reason, we can observe zero values for the applied minimum pressure in the Saint Benoit des Ondes' silt where the probe's resistance is important compared to its limit pressure. This phenomenon is eliminated with the application of the stiffness correction in real time.

3.2.1 Gosier (French Antilles) site

The first field application of the method developed by Dupla in a calibration chamber, was made as part of the Belle-Plaine project on the Gosier Site in the French Antilles (Dupla & Canou, 2010). This site was selected to evaluate liquefaction potential using the cyclic pressuremeter because of its location in this highly seismic area of the Antilles. The site has been investigated using various laboratory, geotechnical and geophysical field experiments including seismic velocity tests, piezocone (CPTu) and cyclic pressuremeter. In addition, boreholes have been drilled to collect samples for physical and mechanical laboratory

Table 1. In situ cyclic pressuremeter tests.

Site	Year	Bore-hole	Depth (m)	Membrane type	PM (MPa)	Pm (MPa)	CSR	N cycles for $\varepsilon_V = 50\%$	Site	Year	Bore-hole	Depth (m)	Index	Membrane type	PM (MPa)	Pm (MPa)	CSR	N cycles for $\varepsilon_V = 50\%$
Gosier	2010	1	4	RM	0.271	0.046	0.35	395	SBdO	2018	1	4		ST	0.160	0.000	0.27	314
Gosier	2010	1	5	RM	0.168	0.001	0.49	257	SBdO	2018	1	5		ST	0.213	0.016	0.21	44
Gosier	2010	1	6	RM	0.225	0.069	0.27	29611	SBdO	2018	2	4		ST	0.132	0.015	0.20	78647
Gosier	2010	1	7	RM	0.216	0.041	0.34	792	SBdO	2018	2	5		ST	0.163	0.000	0.30	17463
Gosier	2010	1	8	RM	0.198	0.014	0.43	9	SBdO	2018	2	6	a	ST	0.333	0.000	0.26	400
Gosier	2010	1	9	RM	0.267	0.071	0.29	289	SBdO	2018	2	6	b	ST	0.465	0.098	0.16	2359
Gosier	2010	1	10	RM	0.278	0.109	0.22	1126	SBdO	2018	2	7		ST	0.377	0.000	0.28	137
Gosier	2010	1	11	RM	0.308	0.140	0.19	547	SBdO	2018	2	8		ST	0.467	0.000	0.28	20
Gosier	2010	2	4	RM	2.128	0.063	0.47	652716	SBdO	2018	2	9		ST	0.268	0.071	0.15	21324
Gosier	2010	2	5	RM	0.214	0.077	0.24	17468	SBdO	2018	3	5		ST	0.161	0.002	0.25	7018
Gosier	2010	2	6	RM	0.191	0.038	0.33	6368	SBdO	2018	3	6		ST	0.189	0.085	0.09	99937
Gosier	2010	2	7	RM	0.182	0.039	0.32	81	SBdO	2018	4	4		ST	0.105	0.000	0.00	11519
Gosier	2010	2	8	RM	0.186	0.015	0.42	18	SBdO	2018	4	5		ST	0.160	0.000	0.47	2726
Gosier	2010	2	9	RM	0.237	0.064	0.29	74	SBdO	2018	4	6		ST	0.192	0.000	0.28	8593
Gosier	2010	2	10	RM	0.256	0.098	0.22	1572	SBdO	2018	4	7		ST	0.305	0.093	0.13	8451
SBdO	2016	1	6	RM	0.247	0.201	0.05	9758	SBdO	2018	4	8		ST	0.334	0.100	0.13	1526
SBdO	2016	1	7	RM	0.235	0.138	0.13	7230	SBdO	2019	3	5		ST	0.279	0.093	0.25	268
SBdO	2016	2	4	RM	0.175	0.106	0.12	3515	SBdO	2019	3	6		ST	0.241	0.097	0.21	3028
SBdO	2016	2	5	RM	0.220	0.115	0.17	479	SBdO	2019	1	4		RM	0.236	0.092	0.22	8
SBdO	2016	2	6	RM	0.239	0.084	0.24	192	SBdO	2019	1	5		RM	0.154	0.085	0.15	116
SBdO	2016	3	4	RM	0.236	0.075	0.26	54	SBdO	2019	1	6		RM	0.205	0.096	0.18	5
SBdO	2016	3	5	RM	0.340	0.088	0.29	25	SBdO	2019	1	7	a	RM	0.258	0.115	0.19	53
SBdO	2016	3	6	RM	0.359	0.096	0.29	5	SBdO	2019	1	7	b	RM	0.145	0.098	0.10	678
SBdO	2016	4	4	RM	0.302	0.071	0.31	2	SBdO	2019	2	5		RM	0.269	0.113	0.20	5
SBdO	2016	4	5	RM	0.248	0.070	0.28	47	SBdO	2019	2	6		RM	0.210	0.089	0.20	70
SBdO	2016	4	6	RM	0.262	0.102	0.22	358	SBdO	2019	2	7		RM	0.176	0.093	0.15	498
SBdO	2016	5	4	RM	0.178	0.075	0.20	194	SBdO	2019	4	5		RM	0.213	0.074	0.24	11
SBdO	2016	5	5	RM	0.140	0.090	0.11	5233	SBdO	2019	4	6		RM	0.276	0.083	0.27	13
SBdO	2016	5	6	RM	0.654	0.018	0.47	13	SBdO	2019	4	7		RM	0.226	0.089	0.22	632
SBdO	2016	6	5	RM	0.257	0.064	0.30	395084	SBdO	2019	4	8	a	RM	0.194	0.102	0.15	649946
SBdO	2016	6	4	RM	0.234	0.000	0.57	8456	SBdO	2019	4	8	b	RM	0.3362	0.108	0.26	11

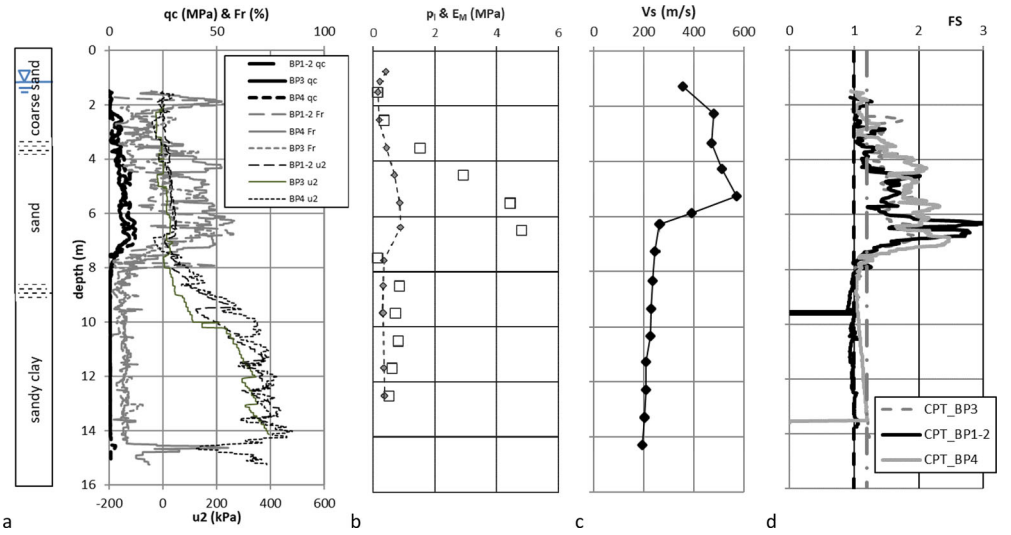

Figure 12. Soil profile at the Gosier site, French Antilles (a) CPT profile (Foray et al., 2008) (b) pressuremeter results (c) shear wave velocity (Foray et al., 2008) (d) factor of safety FS = MSF*CRR7.5/CSR (Youd et al., 2001).

testing and the boreholes were used to install a series of accelerometers and piezometers to monitor future seismic events at the site.

Figure 12 summarizes some of the key indicators of stratigraphy and properties relevant to the liquefaction study obtained from piezocone profiles, pressuremeter testing and seismic shear wave velocity profiling. The CPTU profile suggests that a sandy zone with varying amounts of silt and clay is located between approximately 3 and 8 m overlying a normally consolidated clay layer. The water table was found at about 1.2 m. The sandy zone was further classified using grain size analyses of samples obtained from the various boreholes. Figure 13 shows results from the sieve analyses as summarized by Dupla and Canou (2010) compared to the ranges of grain size distribution for most liquefiable and potentially liquefiable soils proposed by Tsuchida (1970). Using the European standard (CEN, 2004) for liquefaction potential evaluation (Sr = 100%, $Cu = D_{60}/D_{10} < 15$, $0{,}05 < D_{50} < 1.5$ mm), some of the soils shown in Figure 14 were deemed potentially liquefiable according to the ranges established by Kishida (1966) and by Lee and Fitton (1968). Such seismic design codes use protocols to predict the susceptibility of fine-grained soils to liquefaction based solely on the fines content (FC) parameter, which is not sufficient as a single indicator (Bray & Sancio, 2006; Seed et al., 2003). According to these protocols, resistance to liquefaction decreases with decreasing fines content (Youd et al. 2001). However, during recent earthquakes, such as those of Darfield in 2010 and Ecuador in 2016, widespread liquefaction occurred in a significant number of sand deposits with fines content greater than 15%.

A series of monotonic and cyclic Ménard and self-boring pressuremeter tests were conducted at the Gosier site using a probe fitted with a rubber membrane covered with a metallic sheath for the monotonic tests and with a reinforced membrane for the cyclic tests. The metallic sheath was used as protection against the sharp shells present in the soil deposit. The boreholes were advanced by hand using an auger with bentonite injection. The results from the monotonic tests were previously presented on Figure 12 in terms of pressuremeter modulus and limit pressure. The profile of limit pressure shows a clear correlation with the CPT results. The profile of Ménard modulus illustrates the ability of the pressuremeter to perform tests in such variable soil stratigraphy.

Figure 14 shows the results of three cyclic pressuremeter tests performed in the vicinity of the CPTU profiles. Figure 14a shows the pressure corrected for volume accumulation. The results show the increase in volume accumulation as a function of the vertical position in the sandy layer. The tests performed at 8 m depth reached a volume greater than 500 cm^3, which corresponds to a volume deformation close to 100% (or ε_r=41%) for a small number of cycles because of the applied high cyclic ratio (Table 1), while the other tests at 5 and 10 m only accumulated to 60 and 150 cm^3, respectively. The series of curves shown in Figure 14b were approximated by single average curves extrapolated to 100 cycles.

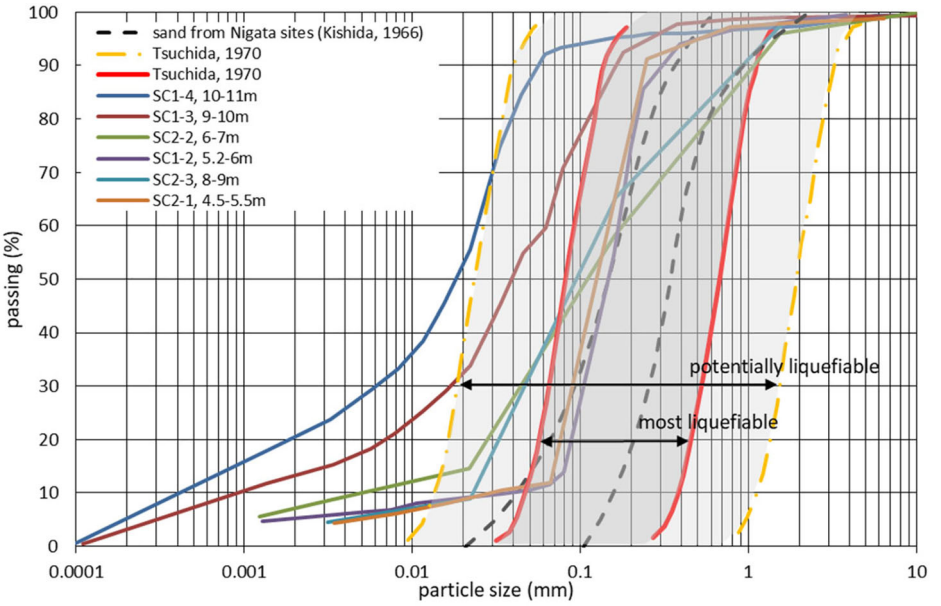

Figure 13. Particle size distribution of granular soils at the Gosier site, French Antilles.

Figure 15 shows the values of the number of cycles at conventional liquefaction as a function of the CSR. These points were obtained by fitting a power law on the accumulation curve envelope previously described. The grouping of results obtained for depths between 5 and 8 m (shown within the ellipse) fits within the classification of less liquefiable soils derived from CPTu results (FS $>$ 1.2).

A power law relationship ($CSR = a.N^b$ with N number of cycles) was used as proposed by Dupla and Canou (2003) to fit a curve on triaxial test results. The results derived from the cyclic pressuremeter tests are in very close agreement to the curve proposed using Eq. (7) (shown as a black solid line curve).

If the 50% volumetric strain is not reached during the test (limited to 50 cycles), the number of cycles at liquefaction is extrapolated using a power law.

The pressuremeter curve was deduced from the triaxial curve using Eq. (7) for a friction angle of 27° and a dense state. In this first campaign, the amplitude was almost kept at the same level but still not corrected during testing. The next test program was designed to investigate the effect of the membrane correction in real-time.

3.2.2. Saint-Benoît-des-Ondes site

The results of a series of cyclic pressuremeter tests performed beneath the Duchess Anne embankment dyke close to the Mont Saint Michel (France) are presented in this section.

The Duchess Anne dike, built between 1020 and 1040, extends from the tip of Château Richeux (south of Cancale), in the west, to the small massif of Saint-Broladre, to the east. The dike separates the marshland from the adjoining sea. The study focused on a 17 km linear section, the management of which is ensured by a local owners' association.

The dike of the Duchess Anne was constructed taking advantage of ancient coastal ridges at this location to protect the Dol marshes from high tidal ranges (15 m tidal range in the bay). The thickness of Quaternary sediments is between 15 and 20 m below the dike and these are essentially made up of pitch (silt size) and fine sands. Given the proximity to the sea and being within the tidal reach, these materials are fully saturated. These marine sands are well-graded. Even if the particle size distribution shown on Figure 16, does not suggest that these soils are liquefiable, their low density leads to a classification by the NCEER CPT method as liquefiable soils (Figure 17).

Figure 17 presents the cone penetration (CPT) profiles obtained on site under the embankment and close to the Ménard pressuremeter tests (MPM) and cyclic pressuremeter tests (PMT) boreholes as well as the shear wave velocity profile (Vs). The water table was found at about 2 m during the tests.

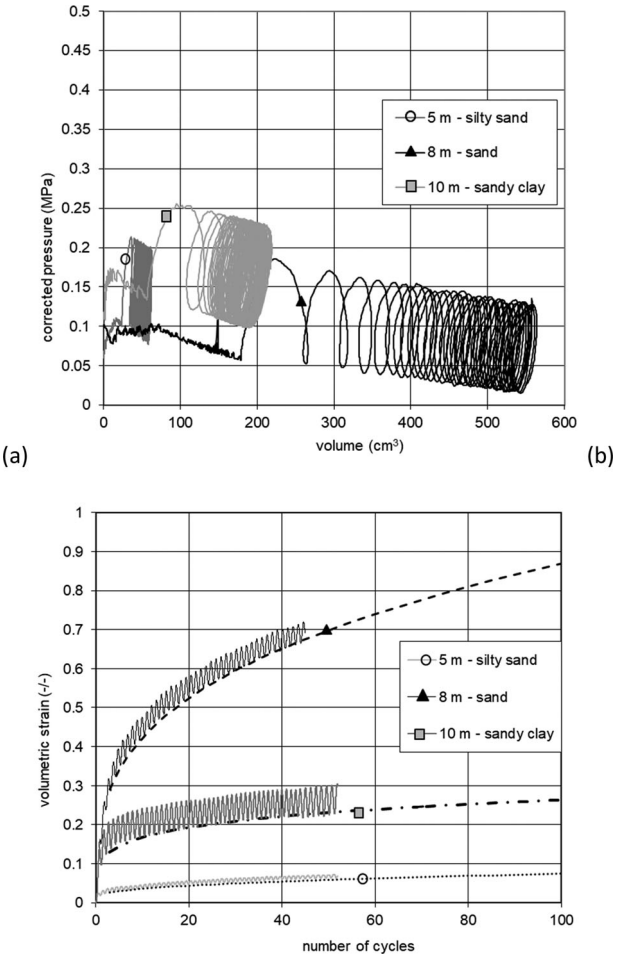

Figure 14. Accumulation curves obtained from the cyclic pressuremeter and envelope curves (borehole 2).

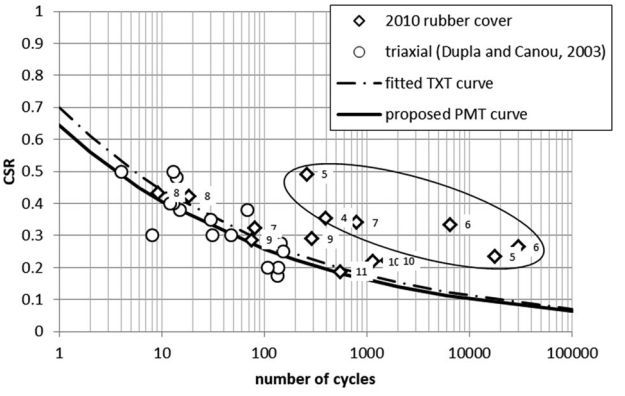

Figure 15. Comparison of CSR-N curve obtained with the triaxial test (dashed line) by (Dupla & Canou, 2010) and cyclic pressuremeter results (symbols with test depth in meters indicated on the right).

The results of the piezocone profiles suggest that the upper layer behaves as a coarse soil (shell sand) overlying a fine silty or somewhat cohesive soil. This was confirmed from observation of samples retrieved when drilling boreholes for pressuremeter tests. Based on the CPT results, the liquefaction threshold proposed by Youd et al. (2001) appears to occur below 3 m depth (Figure 17).

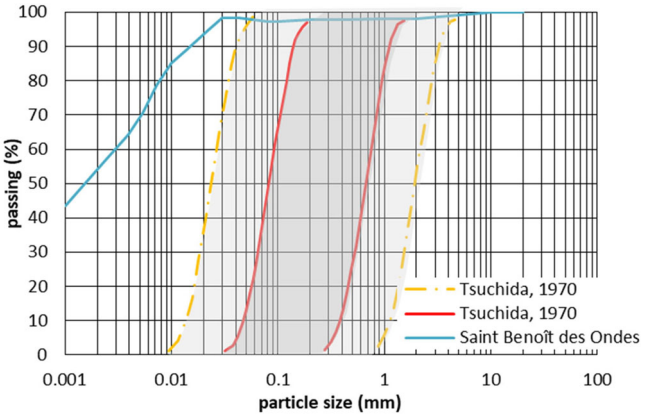

Figure 16. Particle size distribution of silty soil at the Saint-Benoît-des-Ondes site, France.

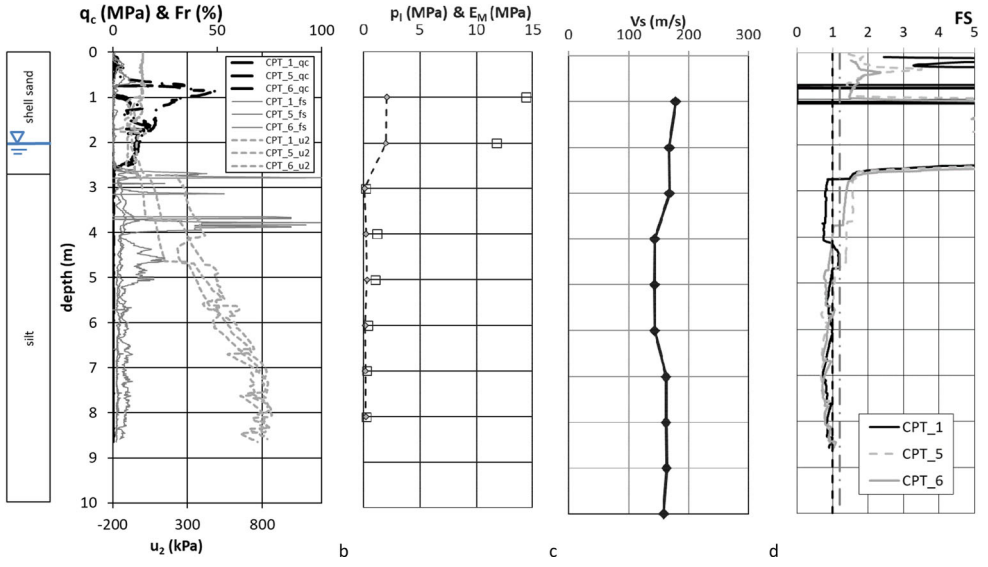

Figure 17. Saint-Benoît-des-Ondes site (a) CPT profile (b) pressuremeter results (c) shear wave velocity (d) factor of safety (Youd et al., 2001).

At the Duchess Anne dike, three separate cyclic pressuremeter test campaigns have been performed: 2016, 2018 and 2019. The analysis of the first set of data obtained during the 2016 campaign showed the need for improvement to achieve the same reliability than in laboratory testing. Changes were made for the 2018 testing, including a first attempt at pore pressure measurements. Figure 18 show the results using two different membrane protection systems.

During these campaigns, the cyclic loading was imposed between two fixed pressure limit set at the surface on the test control device. However, once corrected for membrane stiffness, theses limits were significantly diminished at probe level. To avoid this discrepancy the software was later modified to take into account the pressure loss due to the membrane resistance, in real-time (Figure 7). Once the correction is applied, the pressure at probe level stays almost perfectly constant between the initially defined limits which was not the case for the first two test campaigns in 2016 and 2018.

Figure 18 shows some results from 2019 obtained with the new pressure control approach for both membrane cover systems (i.e. reinforced membrane cover and membrane with slotted tube). The pressure control using the membrane-slotted tube correction appears very efficient even if some slight

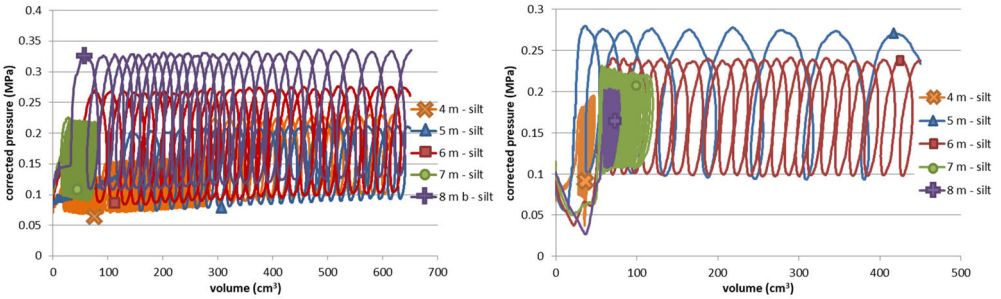

Figure 18. 2019 test campaign – Evolution of pressure with corrected pressure control for probe with (a) rubber membrane (borehole 4) and (b) slotted tube (borehole 3).

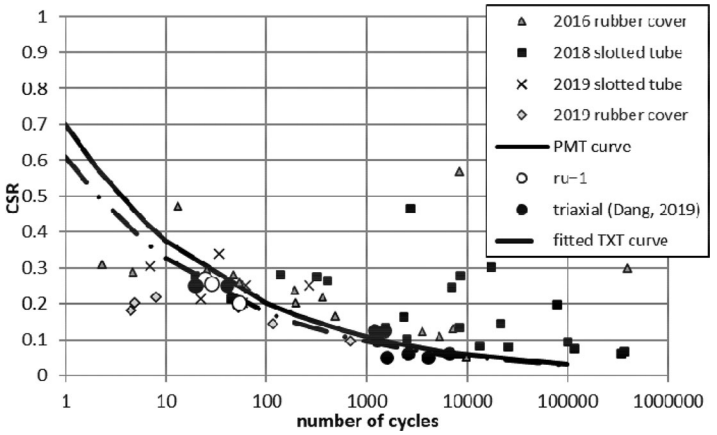

Figure 19. CSR evolution for different cover types.

increase or decrease of the mean pressure is observed. This small variation is attributed to a zero offset from the initial probe volume V_0. In the curves of Figure 18 we observe that the strain accumulates more rapidly as the amplitude of pressure increases, reaching similar volume change for less cycles of unload-reload and corresponds to the behaviour previously observed by Dupla and Canou (2003).

The numbers of cycles to the conventional failure, according to the CSR applied to all tests of all 3 campaigns, are summarized on Figure 19. The results show that the points obtained during the three campaigns are close together and as anticipated, the difference appears to be for the highest number of cycles, i.e. for a higher volume and thus a higher influence of the pressure loss. Data from the 2016 and 2018 campaign obtained using the old control approach as well as a rubber membrane and slotted tube are more scattered than the corrected data of the 2019 campaign with both membrane covers. Due to the decrease of the two pressure limits (upper and lower) during the first two campaigns, the actual CSR increases but the mean pressure decreases significantly during the test.

All the results give a clear trend close to the curve fitted on cyclic triaxial test results performed on reconstituted specimens and the proposed pressuremeter curve for a friction angle of 22°.

3.3. Pore pressure evolution

During the last test campaign (2019), measurements of pore pressure during the cyclic loading have been performed at mid-height of the probe as shown previously on Figures 3 and 4. Figure 20 show the evolution of pore water pressure measured directly on the probe during the tests in borehole 4 at different depths. The response of the signal is a good indication that the transducer was working as intended. The increase in pore pressure follows the increase in the pressure cycle amplitudes.

As an initial approach, a comparison of an *in situ* pore pressure ratio similar to r_u (Eq. (10)) for the triaxial test, has been made as shown on Figure 20. As for the CSR calculation (Eq. (4)), the effective

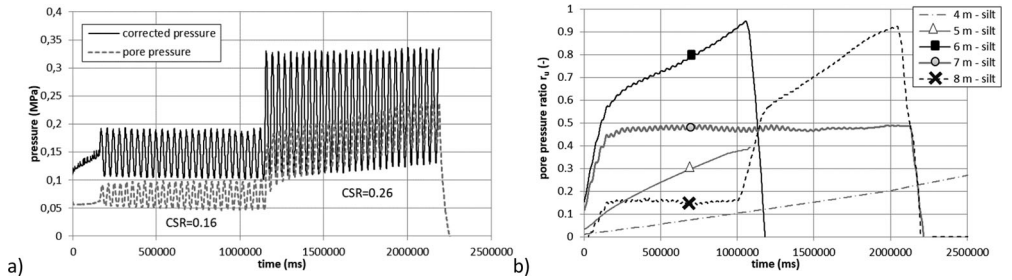

Figure 20. Example of a) pore pressure measurement during Saint-Benoît-des-Ondes test campaign (membrane cover, 8 m depth) b) in situ ru ratio evolution during cycling.

confinement stress is considered as the effective mean accumulation pressure.

$$r_u = \frac{\Delta u}{\sigma'_{H;mean}} = \frac{\Delta u}{\frac{p_M + p_m}{2} - u_o} \tag{10}$$

When r_u reaches a value close to 1, the soil resistance drops dramatically as shown in Figure20. With this additional measure, the cyclic pressuremeter can provide a reliable alternative to triaxial testing and be performed in situ. Either the radial strain threshold or the pore pressure ratio may be used to define the liquefaction of the soil surrounding the probe (Figure 19).

4. Conclusions

In this paper a new ground investigation procedure to evaluate the cyclic resistance based on multicyclic pressuremeter testing has been presented. The interpretation of results may be performed similarly to what is done in laboratory triaxial testing. The results suggest that a CSR curve can be proposed without the need for sampling and laboratory testing on disturbed or reconstituted samples, especially in cohesionless soils.

Once the appropriate membrane loss corrections were applied to the pressure control system, the proper test procedures keep the pressure applied to the soil defining the cycles constant and lead to measurements of pore pressures which showed a progression in agreement with the volumetric strain measurements from the accumulated unload-reload cycles. The addition of pore pressure measurements provides new perspectives on the study of the liquefaction risk potential by observing the fluctuations of the coefficient r_u when applying cyclic loading in situ.

Acknowledgement

The authors thank the national project ARSCOP, ANR project Belle Plaine (grant ANR-06-CATT-003) and ISOLATE (grant ANR-17-CE22-0009) and the French Ministry of Ecological Transition for funding this research project, Jean Lutz SA company and ANRT for funding Mr Karagiannopoulos' thesis as well as their colleagues R. Benot, G. Desanneaux, O. Malassingne and F. Szymkiewicz for assisting in this project.

Disclosure statement

No potential conflict of interest was reported by the authors.

References

AFNOR. (1999). Ground investigation and testing, Ménard pressuremeter test – part 2 test with one cycle NF P94-110-2. (pp. 43, In French).

ASTM. (2020). Standard Test Methods for Prebored Pressuremeter Testing in Soils ASTM D4719. 13.

Benoît, J., Reiffsteck, P., & Getchel, A. (2020). *In situ empirical determination of earth pressures at-rest [Paper presentation]*. 6th Int. Conf Geotechnical and Geophysical Site Charac., Budapest Hongrie, 8.

Bensaïd, A. (1985). *In-situ measurements of pore pressures. Application to soil investigation* [PhD Géologie appliquée]. École Nationale des Ponts et Chaussées. 399. (In French)

Bray, J. D., & Sancio, R. B. (2006). Assessment of the liquefaction susceptibility of fine-grained soils. *Journal of Geotechnical and Geoenvironmental Engineering*, *132*(9), 1165–1177. https://doi.org/10.1061/?ASCE?1090-0241?2006?132:9?1165

Castro, G. (1975). Liquefaction and cyclic mobility of saturated sands. *Journal of the Geotechnical Engineering Division*, *101*(6), 551–569. https://doi.org/10.1061/AJGEB6.0000173

CEN. (2004). *Eurocode 8: Design of structures for earthquake resistance – Part 5: Foundations, retaining structures and geotechnical aspects, European Committee for Standardization*., CEN, Brussel. 45.

Combarieu, O., & Canépa, Y. (2001). The unload-reload pressuremeter test. *Bulletin des Laboratoires des Ponts et Chaussees*, *233*, 37–65.

Dang, Q. H. (2019). *Soil behaviour under artificial liquefaction, improvement of soils with liquefiable risks* [PhD thesis]. Université Paris-Est. 238. (In French)

Dupla, J. C., & Canou, J. (2003). Cyclic pressuremeter loading and liquefaction properties of sands. *Soils and Foundations*, *43*(2), 17–31. https://doi.org/10.1016/S0038-0806(20)30800-3

Dupla, J. C. (1995). *Application of the cylindrical cavity expansion to the evaluation of the liquefaction potential of sand* [PhD thesis]. Ecole nationale des Ponts et Chaussées. 423. (In French)

Dupla, J. C., & Canou, J. (2010). *Belle-Plaine: study of liquefiable soils under real conditions; pilot site and predictive models, Ecole des Ponts ParisTech, (CERMES), Belle plaine ANR project report*. 45. (In French)

Ferreira, C., Viana da Fonseca, A., Ramos, C., Saldanha, A. S., Amoroso, S., & Rodrigues, C. (2020). Comparative analysis of liquefaction susceptibility assessment methods based on the investigation on a pilot site in the greater Lisbon area. *Bulletin of Earthquake Engineering*, *18*(1), 109–138. https://doi.org/10.1007/s10518-019-00721-1

Foray, P., Rousseau, C., Barnoud, J.-M., & Santruckowa, H. (2008). *Piezocone investigation and installation of pore pressure sensors on the Gosier site, Univ. Grenoble (3SR), Belle plaine ANR project report*. 41. (In French)

Gobbi, S. (2020). *Characterization of liquefaction parameters for saturated soil under dynamic loading using laboratory tests and calibration of constitutive laws by numerical modelling* [PhD thesis]. University Gustave Eiffel. 240.

Ishihara, K. (1993). Liquefaction and flow failure during earthquakes. *Géotechnique*, *43*(3), 351–415. https://doi.org/10.1680/geot.1993.43.3.351

ISO. (2004)., Geotechnical investigation and testing. Field testing. Ménard pressuremeter test, EN ISO 22476-4. pp. 43.

Jaky, J. (1944). The coefficient of earth pressure at rest. Magyar Mernok es Epitesz-Egylet Kozlonye. (In Hungarian, 355–358).

Jézéquel, J. F., & Le Méhauté, A. (1982). *Cyclic tests with self-boring pressuremeter, symposium on the pressuremeter and its marine applications*. ISP2. pp. 221–233.

Karagiannopoulos, P. G. (2020). *Contribution of the interstitial pressure measurement to the determination of the parameters of the behaviour laws in monotonic and cyclic expansion tests* [PhD thesis]. Université Gustave Eiffel. (In French)

Kishida, H. (1966). Damage to reinforced concrete buildings in Niigata City with Special reference to foundation engineering. *Soils and Foundations*, *6*(1), 71–86. https://doi.org/10.3208/sandf1960.6.71

Lee, K. L., & Fitton, J. A. (1968). Factors affecting the dynamic strength of soil. American Society for Testing and Materials, STP 450, ASTM, Vibration Effect on Soils and Foundations,

Little, R. L., & Briaud, J. L. (1988). A pressuremeter method for single piles subjected to cyclic lateral loads in sand. Miscellaneous paper GL-88-14.

Masuda, K., Tsukamoto, Y., & Ishihara, K. (2008). Some recent findings in evaluating stress-strain properties of sandy soils from pressuremeter. In H. Mayne (Ed.), *Geotechnical and geophysical site characterization, ISC-3* (pp. 1099–1104). Taylor & Francis Group.

Masuda, K., Nagatoh, R., Tsukamoto, Y., & Ishihara, K. (2005). *Use of cyclic pressuremeter with multiple cells for evaluation of liquefaction resistance of soils*., ISP5, Presses des Ponts Ed.

Ménard, L. (1960). Unloading phase of pressuremeter test, Theoretical study and application, Circulaire 24/60, TLM. 3. (In French)

Mokrani, L. (1991). *Physical simulation of the behaviour of piles at great depths in a calibration chamber* [PhD thesis]. Institut national Polytechnique de Grenoble. 307. (In French)

Reiffsteck, P., Saussaye, L., & Habert, J. (2020). *Borehole quality influence on expansion test results*, ISC6.

Seed, R. B., Cetin, K. O., Moss, R. E. S., Kammerer, A. M., Wu, J., Pestana, J. M., Riemer, M. F., Sancio, R. B., Bray, J. D., Kayen, R. E., & Faris, A. (2003). Recent advances in soil liquefaction engineering: a unified and consistent framework. *Proceedings of the 26th Annual ASCE Los Angeles Geotechnical* Spring.

Tani, K. (1995). *General report: Measurement of shear deformation of geomaterials. – Field tests, 1er Int. Symp. on Prefailure deformation of geomaterials*. Balkema, 1115–1131.

Tatsuoka, F., Jardine, R. J., Lo Presti, D., & Di Benedetto, H. (1997). *Characterising the prefailure deformation properties of geomaterials [Paper presentation].* Proceedings, 14th International Conference on Soil Mechanics and Foundation Engineering, Hamburg, vol. 4, 2129–2164.

Tsuchida, H. (1970). Evaluation of liquefaction potential of sandy deposits and measures against liquefaction induced damage. In *Proceedings of the Annual Seminar of the Port and Harbour Research Institute* (pp. 3–1–3-33). (in Japanese).

Ueno, K., Mohri, Y., Tanaka, T., & Tatsuoka, F. (2015). *Effect of initial shear stress on strength reduction of compacted soil during undrained cyclic loading 25th ICOLD*., Stavanger. 286–304

Vernay, M., Morvan, M., & Breul, P. (2020). Experimental study on the influence of saturation degree on unstable behavior within granular material. *European Journal of Environmental and Civil Engineering*, *24*(11), 1821– 1819. https://doi.org/10.1080/19648189.2018.1488623

Youd, T. L., Idriss, I. M., Andrus, R. D., Arango, I., Castro, G., Christian, J. T., Dobry, R., Finn, W. D. L., Harder, L. F., Jr., Hynes, M. E., Ishihara, K., Koester, J. P., Liao, S. S. C., Marcuson, W. F., III Martin, G. R., Mitchell, J. K., Moriwaki, Y., Power, M. S., Robertson, P. K., Seed, R. B., & Stokoe, K. H. II (2001). Liquefaction resistance of soils: Summary report from the 1996 NCEER and 1998 NCEER/NSF Workshops on Evaluation of Liquefaction Resistance of Soils. *Journal of Geotechnical and Geoenvironmental Engineering*, *127*(10), 817–833. 2001: https://doi.org/10.1061/(ASCE)1090-0241(2001)127:10(817)